Crucial role of Fe in determining the hard magnetic properties of Nd$_2$Fe$_{14}$B

Juba Bouaziz[*]

Department of Physics, University of Warwick, Coventry CV4 7AL, UK and
Peter Grünberg Institut and Institute for Advanced Simulation,
Forschungszentrum Jülich & JARA, D-52425 Jülich, Germany

Christopher E. Patrick

Department of Materials, University of Oxford, Parks Road, Oxford OX1 3PH, UK

Julie B. Staunton[†]

Department of Physics, University of Warwick, Coventry CV4 7AL, UK
(Dated: January 5, 2023)

Nd$_2$Fe$_{14}$B's unsurpassed, hard magnetic properties for a wide range of temperatures result from a combination of a large volume magnetization from Fe and a strong single-ion anisotropy from Nd. Here, using finite temperature first-principles calculations, we focus on the other crucial roles played by the Fe atoms in maintaining the magnetic order on the Nd sublattices, and hence the large magnetic anisotropy, and directly generating significant uniaxial anisotropy at high temperatures. We identify effective spins for atomistic modelling from the material's interacting electrons and quantify pairwise and higher order, non-pairwise magnetic interactions among them. We find the Nd spins couple most strongly to spins on sites belonging to two specific Fe sublattices, $8j_1$, $8j_2$. Moreover the Fe $8j_1$ sublattice also provides the electronic origin of the unusual, nonmonotonic temperature dependence of the anisotropy of Y$_2$Fe$_{14}$B. Our work provides atomic-level resolution of the properties of this fascinating magnetic material.

The elemental lanthanides show remarkable magnetic properties deriving from their partially-filled shells of atomic-like $4f$ electrons. However, direct exploitation of these properties is hindered by low magnetic ordering temperatures. No elemental lanthanide retains its magnetism at room temperature, with the highest Curie temperature T_c being 292 K for Gd [1]. Combining the lanthanides with other elements can strengthen the magnetic interactions and allow ordering to persist to higher temperatures. The most successful example of this paradigm is the rare-earth/transition-metal (RE-TM) family of permanent magnets [2]. Specifically, Nd-Fe-B demonstrates exceptional magnetic strength over a wide range of temperatures. Having revolutionized computer hard disk technology in the last century, Nd-Fe-B is again under intense investigation owing to its use in electric vehicle motors and renewable energy turbines [3].

The RE-TM magnetic interactions are most simply described in terms of the exchange field $\boldsymbol{B}_{\text{exch}}$. In this picture, the TM-$3d$ electrons produce an effective magnetic field which couples to the spin magnetic moments of the RE ions. A minimal model to describe the RE ions and the high magnetic anisotropy they generate combines this exchange field with the interaction with an external field $\boldsymbol{B}_{\text{ext}}$ and the crystal field $\hat{V}_{\text{CF}}$, which describes the (predominantly) electrostatic interaction of the $4f$ charge cloud with its environment [4–7]:

$$\mathcal{H}_{\text{RE}} = 2\mu_B\,\hat{\boldsymbol{S}} \cdot \boldsymbol{B}_{\text{exch}} + \mu_B\,(\hat{\boldsymbol{L}} + 2\hat{\boldsymbol{S}}) \cdot \boldsymbol{B}_{\text{ext}} + \hat{V}_{\text{CF}}. \quad (1)$$

$\hat{\boldsymbol{S}}$ and $\hat{\boldsymbol{L}}$ are the total spin and orbital angular momentum operators. Values of the exchange field can be extracted by fitting Eq. 1 to experimental data obtained in inelastic neutron scattering (INS) or magnetization measurements. Experimental estimates of $\boldsymbol{B}_{\text{exch}}$ are far stronger than fields achievable in the laboratory ($\mu_B B_{\text{exch}}/k_B \gtrsim 300\ K$ [8], i.e. $B_{\text{exch}} \gtrsim 450$ T) as required to maintain magnetic order above room temperature.

Going beyond a phenomenological understanding of RE ordering requires an atomistic picture of the magnetic interactions among effective spins. Nd$_2$Fe$_{14}$B has a tetragonal crystal structure with 68 atoms per unit cell ([8] [9]). The RE atoms occupy two crystallographically distinct sites (RE$_{4f}$ and RE$_{4g}$), which (together with Fe$_{4c}$ and B$_{4g}$ atoms) form planes encapsulating the remaining 5 Fe sublattices ($4e$, $8j_1$, $8j_2$, $16k_1$, $16k_2$). For the Nd sites the spins come from the localized f-electrons but for the TM sites the local effective spins, or local moments, emerge from the material's itinerant electron fluid [10]. Spin-polarized regions at atomic sites form from co-operative behavior of the valence electrons and at finite temperatures their orientations fluctuate on relatively long time scales compared to the remaining electronic degrees of freedom. These local magnetic moments are the pertinent, effective spins for the TM aspect of the atomistic modelling.

A conceptually simple model assumes interactions only between pairs of spins (ij) according to the classical Heisenberg model, $-\mathcal{J}_{ij}\hat{\boldsymbol{S}}_{\boldsymbol{i}} \cdot \hat{\boldsymbol{S}}_{\boldsymbol{j}}$ where $\hat{\boldsymbol{S}}_{\boldsymbol{i}}$ represents an effective spin. Previous works [12, 13] calculate such $\mathcal{J}_{ij}$ parameters from first principles within density-functional theory (DFT) [12, 13], and use them directly in atomistic spin dynamics simulations. With the TM magnetocrystalline anisotropy (MCA) modelled as a sum of single
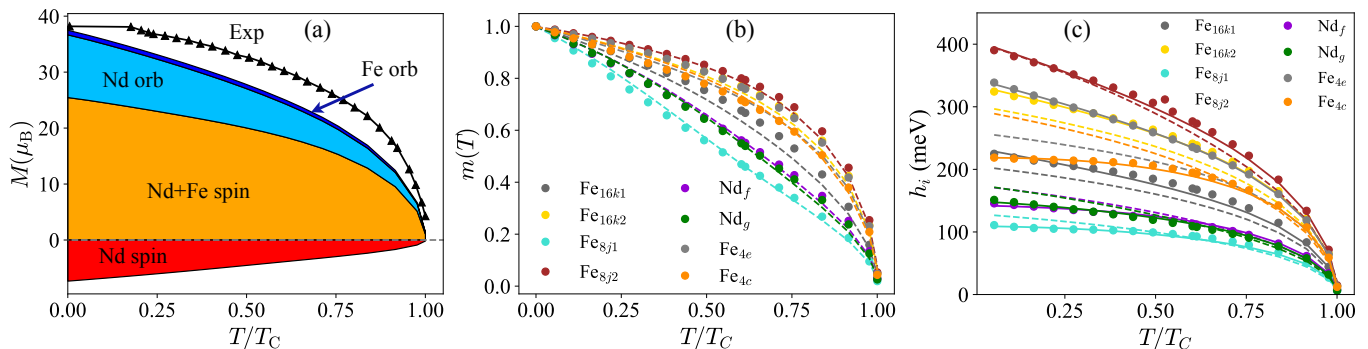
FIG. 1. (a) Nd$_2$Fe$_{14}$B's magnetization versus (T/T_c) from DLM-DFT calculations compared to experiment [11]. (b) Sub-lattice resolved magnetic order parameters and (c) Weiss fields. The dots indicate the full DLM-DFT results, dashed lines from a pair-wise interaction model and continuous lines from a fit of the DLM-DFT results to the model discussed in the text Eq. (3).

ion-like terms, assumed to be substantial, and RE crystal field coefficients taken from experiment, the simulations can reproduce the magnetization behavior of Nd$_2$Fe$_{14}$B, including the spin reorientation transition at low temperature, and represent the current state-of-the-art in modelling these magnets [14]. Although such a pair-wise Heisenberg model is computationally straightforward to implement, it is nonetheless a clear presumption for a magnetic metal like Nd-Fe-B. Despite the huge technical importance of the material, the role of "beyond Heisenberg" itinerant electron spin features has yet to be elucidated for Nd-Fe-B. Moreover the MCA from the spin-orbit coupling of the itinerant d-electrons is also not guaranteed to be single-ion like [15]. In this letter we quantify the significance of both these aspects and propose ways to improve atomistic spin modelling.

The disordered local moment (DLM) picture implemented within DFT provides an appropriate *ab initio* framework [10, 15, 16]. The approach combines statistical mechanics of the effective spins (local moments, $\{e_i\}$) and DFT, to describe the complementary evolution of electronic and magnetic structure as a material's temperature is varied. Strongly correlated 4f-electron effects are treated with a parameter free, self interaction correction (SIC) approach [17, 18] which incorporates Hund's rules naturally [19]. As such DLM-DFT can describe temperature-dependent magnetic properties of permanent magnets as shown recently for the RECo$_5$ family [7]. The crucial RE contribution to the anisotropy is accounted by crystal field theory, calculating the CF coefficients within DFT using a robust numerical method [16] so that the modelling is independent of any prior fit of phenomenological parameters.

Here we investigate the nature of magnetic order in Nd$_2$Fe$_{14}$B, sublattice-resolved, and describe the magnetic interactions among the effective spins associated with both RE and TM sites. We show that the interactions among the TM spins are influenced by the global magnetic order and its impact and link with the spin-

polarised electrons of the system. This is in essence a multi-spin coupling effect. We find significant diversity in the behavior of the Fe local moments depending on their location in the unit cell. While most TM spins are ferromagnetically-coupled, some interact antiferromagnetically with each other. This leads to some frustration and a peculiar strong suppression of magnetic order on the $8j_1$ sites which are located roughly midway between the Nd-containing layers. We also find that the Nd spins couple most strongly to spins on sites belonging to this Fe sublattice along with those on another ($8j_2$). Furthermore we discover a link between this $8j_1$ sublattice and the unusual non-monotonic temperature dependence of the non-RE MCA of the isostructural material Y$_2$Fe$_{14}$B, resolving a longstanding a puzzle [11, 20]. Finally our calculation of the anisotropy field of Nd$_2$Fe$_{14}$B across a range of temperatures agrees well with experiment and confirms the vital role played by the Fe spins for the functionality of this champion magnet.

Apart from the local moments themselves, the central quantities in DLM-DFT theory are Weiss fields $\{h_i\}$ which, analogously to the exchange field of Eq.1, drive the ordering of the local moments. However, unlike B_{exch}, the Weiss fields are not phenomenological, but instead are rigorously defined by thermal averages over the local moment orientational configurations $\{e_i\}$ of the magnetic energy $\Omega\{e_i\}$ [10, 15], i.e.

$$h_i = \int \frac{3}{4\pi} \langle \Omega \rangle_{e_i;T}\, de_i \ . \qquad (2)$$

where $\langle X \rangle_{e_i}$ denotes the average of X with the restriction that the orientation of the moment on site i is fixed as e_i and the order parameters of the local moments, $\{m_i\}$ are the averages $\{\langle e_i \rangle\}$ [10, 15]. $\langle \Omega \rangle_{\hat{e}_i;T}$ is calculated from DFT [10]. Crucially no prior prescription is assumed for the form of the magnetic interactions inherent in the first-principles Ω. For a pairwise Heisenberg model, the magnetic energy $\Omega\{e_i\} = -1/2 \sum_{ij} \mathcal{J}_{ij} e_i \cdot e_j$ with Weiss fields linear in the $\{m_i\}$, $h_i = \sum_j \mathcal{J}_{ij} m_j$.
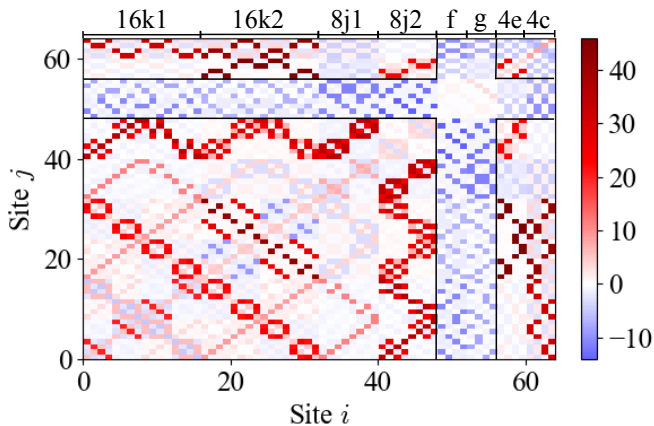
FIG. 2. The relative strengths of interactions between sites in the unit cell (boron sites not included), $\mathcal{J}_{ij}$, (Eq. 3) highlighting the RE-TM ones (sites 48–51 and 52–55 correspond to $4f$ and $4g$ respectively). Numerical values in meV are given in [9] along with specific site coordinates. Red/blue color indicates FM/AF interactions.

Consequently beyond-pairwise terms are clearly identified in DLM-DFT theory from the non-linear dependence of the Weiss fields on the $\{m_i\}$ [21–25]. The $\{m_i\}$ order parameters, describing an equilibrium state at a temperature T, are given by the self-consistent solution of Eq.2 and $m_i = (-1/\beta h_i + \coth \beta h_i)$, the Langevin function, $(\beta = 1/k_B T)$.

Figure 1(a) shows the magnetization as a function of T compared to experiment and resolved into the RE and TM spin and orbital components. The magnetization is directed along $\theta = 45°$ in the (xz)-plane. Full calculational details are given in the Supplemental Material [9] and references [16, 26–28]. The contribution from a particular site i is found by multiplying its local moment magnitude, μ_i, by the order parameter $\boldsymbol{m}_i(T)$. The Fe and Nd spin moments interact antiferromagnetically (AF) and order in an anti-parallel alignment in a ferrimagnetic state, but the large orbital moment of Nd, pointing opposite to its spin, leads to overall ferromagnetic (FM) order. The Fe orbital moments are small ($\sim 0.05\mu_B$/atom). The calculated T_c is 1058 K, which, although an overestimate of 473 K in comparison to the experiment [11], is reasonable for a first-principles theory which uses a mean field approximation for the statistical mechanics of the effective spins [28].

On each of the six Fe and two Nd sublattices ([8, 9] the magnetic order varies from complete, $\{m_i = 1\}$, at $T = 0$K to zero above T_c, $\{m_i = 0\}$. Figure 1(b) shows how the temperature dependence of magnetic order varies across the sublattices. The Nd sublattices disorder more quickly than all the Fe sublattices except the $8j_1$ one. Complementary information in Fig. 1(c) shows that Weiss fields, $\{h_i\}$, promote strong ordering when large and have considerable sublattice variation,

notably the factor ~4 difference between the $8j_1$ and $8j_2$ sites. Analysis of $\{h_i\}$, Eq.2, reveals the presence and importance of interactions that fall outside those of a Heisenberg-like model. For such a pairwise model the $\mathcal{J}_{ij}$ interactions (Fig. 2), directly obtained from the Weiss fields for small values of the $\{m_i\}$, are used to construct the model's Weiss fields and $\{m_i\}$ at all T (dashed lines in Fig. 1(c)). There are large discrepancies from the full *ab initio* DLM-DFT data away from T_c, leading us to propose a more realistic representation of the interactions which is straightforward to incorporate into atomistic spin modelling of the magnet's properties. It leads to a magnetic energy per unit cell

$$\bar{\Omega} = -\frac{1}{2}\sum_{ij} \mathcal{J}_{ij}\boldsymbol{m}_i \cdot \boldsymbol{m}_j - \frac{1}{4}\sum_i \mathcal{B}_I(\boldsymbol{m}_i \cdot \boldsymbol{M})^2, \quad (3)$$

where i, j run over the sites in the unit cell, I denotes one of the 8 sub-lattices to which the site i belongs and $\boldsymbol{M}$ is the total magnetization per unit cell, $\boldsymbol{M} = \sum_i \mu_i \boldsymbol{m}_i$ where the order parameters on the RE sites are antiparallel to the TM sites for the ferrimagnetic state. The second, higher order term captures the effect of the overall spin-polarization of the electronic structure on the effective interactions between the local moments. Computing Weiss fields from this expression fits the DLM-DFT calculations very well as shown by the full curves in Fig. 1(c) and $\bar{\Omega}$ closely approximates $\langle\Omega\rangle_T$. Table I lists the $\mathcal{B}_I$ parameters that measure the sublattice-dependent size of these higher order, multi-spin terms.

System	$4c$	$4e$	$8j_1$	$8j_2$	$16k_1$	$16k_2$	R_f	R_g
Nd$_2$Fe$_{14}$B	-15.42	14.31	-5.06	-1.38	3.82	4.44	-2.53	-1.41
Y$_2$Fe$_{14}$B	-13.68	9.91	-4.07	1.27	4.25	4.07	0.0	0.0

TABLE I. Effective, multi-spin interaction constants (in μeV), $\mathcal{B}_I$, for Nd$_2$Fe$_{14}$B and Y$_2$Fe$_{14}$B.

Fig. 2 shows the relative strengths of the $\mathcal{J}_{ij}$ interactions between pairs of sites. They are represented on a 64×64 grid (56 Fe sites and 8 RE sites and arranged according to sublattice). Numerical values are given as Supplemental Material [9]. Assuming a range less than roughly 5Å, they can be directly used in atomistic spin simulations together with the terms from Table I. The figure illustrates the vital importance on the RE magnetic ordering of the hexagonal nets of Fe atoms [8, 9] from the k_1, k_2 and notably sites on the j_1 and j_2 sublattices. Indeed the largest contributions to the Weiss fields at the RE sites originate from the j_1 and j_2 sublattices.

The TM-TM interactions are particularly varied ranging from FM (red) for the majority to AF (blue). The j_1 sites have AF interactions with e, c and RE sites and strong FM ones with j_2 sites. This frustration drives this sublattice's aversion to magnetic order. The diversity of the interactions stems from the profound effect

that atom coordination and spacing of Fe atoms in a metallic material has on its magnetism. The archetype for this quintessentially itinerant electron effect is fcc Fe where squeezing the lattice turns ferromagnetic order anti-ferromagnetic and then destroys it [29, 30].

The diverse nature of the magnetic order on the six Fe sub-lattices also has an impact on the intrinsic MCA generated by the system's itinerant valence electrons. As found for other TM metal magnets [15, 26], a simple fit in terms of a single ion model is unsatisfactory and, as found for other itinerant electron magnets, two-ion type terms should be included in the model [15, 31, 32]. Furthermore, on general grounds, modelling the MCA as a sum of single ion anisotropy terms must be done extremely carefully. The various Fe sites have different crystallographic point symmetries, and their unique symmetry axes do not necessarily point along the c direction [33]. There are important implications for atomistic spin dynamics simulations [14, 31, 34] where it is not correct to assign a single ion anisotropy to each Fe atom with the same angular dependence and same symmetry axes. Rather a simpler and more rigorous alternative would be to compute an anisotropy energy based on the vector sum of all moments in the same sublattice so that a single symmetry axis is recovered [5].

While significantly smaller than from the f-electrons of the Nd atoms, the primarily TM component of the MCA grows in importance with rising T. As the RE MCA drops swiftly along with the magnetic order [35, 36], the TM contribution can actually increase as shown explicitly in measurements on $Y_2Fe_{14}B$ [11, 20]. Such non-monotonic temperature variation is puzzling, and has been attributed to a magnetostructural effect from an anisotropic expansion of the crystal lattice, competing single-ion-like contributions [20] or competing single and two-ion MCA using atomistic spin dynamics simulations [31, 32] Since fully relativistic effects such as spin-orbit coupling are included in our DLM-DFT theory we investigate the MCA temperature dependence directly and show our results in Fig. 3 for $Y_2Fe_{14}B$.

Using the highly accurate, full potential (FP) KKR code [37, 38], we first calculate the MCA at $T = 0K$ to be ≈ 0.9 meV/formula unit (FU) which agrees well with experimental values [11]. The same rapid loss of magnetic order with increasing temperature which we find for the Fe $8j_1$ sites in $Nd_2Fe_{14}B$ (Fig. 1(b)) is also evident in $Y_2Fe_{14}B$ [9] and this points to a significant role for this sublattice in the anomalous MCA T-dependence. We therefore carry out further FP MCA calculations where now the Fe $8j_1$ sites are constrained to be magnetically disordered ($m_{8j_1} = 0$) via an equal weighting of local moments on each of these sites along the $\pm x$ and $\pm z$ directions. The effect on the computed MCA is striking - it increases greatly to ≈ 1.7 meV/FU - and we infer that the much faster decrease of $8j_1$ magnetic order with temperature relative to that on the other Fe sublattices

is the key driver for the MCA T-dependence.

To test this proposition, we calibrate DLM-DFT MCA values against our $T = 0K$ FP MCA calculations, given the current implementation with an atomic sphere approximation (ASA). Although the ASA values are smaller than the FP ones, the same large increase of the value when the Fe $8j_1$ sites are magnetically disordered is found. In Fig. 3 we show the DLM-DFT temperature dependent MCA both using the ASA (red curve) and also scaled by the ratio between the FP and our ASA $T = 0K$ values (green). The increase with temperature is evident, peaking at $T/T_c = 50\%$ in line with experiment [11] confirming our proposition. Since the calculations are for a fixed lattice structure, we can exclude thermal expansion as a cause of the non-monotonic behavior. We also show the effect on the MCA of forcing the Fe_{8j_1} sublattice to remain magnetically disordered at all T, i.e. $m_{8j_1} = 0$. The resulting unscaled MCA, shown in black in Fig. 3, is dramatically altered - the peak has gone and the MCA decays linearly with temperature and the $T = 0K$ value is enhanced significantly. Clearly, establishment of magnetic order on the $Fe8j_1$ sublattice correlates with a substantial drop in the (uniaxial) MCA.
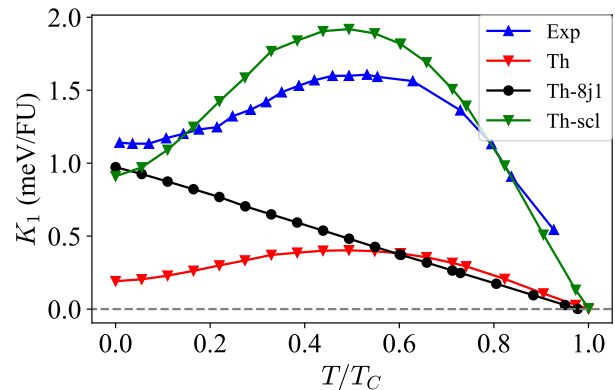

FIG. 3. The T-dependence of the leading anisotropy constant, K_1, of $Y_2Fe_{14}B$ from DLM-DFT theory (red curve) and experiment (blue) [11]. The green curve shows the theory values, scaled to account for the difference between FP [37] and ASA ([9]) at $T = 0K$. The black curve shows K_1 (unscaled) if the Fe $8j_1$ sublattice is constrained to be disordered magnetically.

Our ultimate goal is to describe $Nd_2Fe_{14}B$'s large magnetic anisotropy and its temperature variation. So to the TM MCA we add the dominant RE components. These are calculated [6, 39] from the solution of Eq. 1 where the crystal field coefficients [9] are determined from first principles [16], and exchange field, $\boldsymbol{B}_{exch}$ provided directly by the DLM-DFT Weiss field for each Nd site (Fig. 1) divided by the computed Nd spin moment of 3.66 μ_B.

Our calculated exchange fields of 699 and 725 T for the RE f and g sites respectively are somewhat larger than those used in fits of experimental magnetization
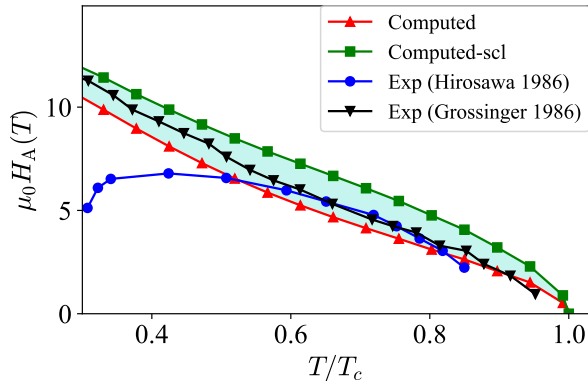
FIG. 4. Evolution of the anisotropy field, H_A, versus T/T_c from theory compared to experimental measurements (from Refs. [42], black curve, [11], blue curve). The agreement is good above $T_c/2$. The red and green curves use the non-RE MCA taken from the red and green curves of Fig. 3.

data (450–520 T [40]), but as pointed out in Ref. [8], the large number of parameters in Eq. 1 introduce significant uncertainties. In principle, INS data would provide a direct measure of the exchange fields but are not available for Nd-Fe-B. Our proposed values are, however, supported by the good agreement between INS experiments [41] and our DLM-DFT calculations for the related $Gd_2Fe_{14}B$ magnet (324 T vs 307/319 T). The Gd exchange fields are substantially smaller than those calculated for Nd. The relative difference ($\sim$2) mirrors that of the spin moments (7.46 vs. 3.66 μ_B) and reflects the similar Weiss fields we calculate for the two materials.

Using the method of Ref. [39] we calculate effective anisotropy constants $K_1(T)$, $K_2(T)$ and anisotropy field, $\mu_0 H_A = 2K_1/M$ *ab initio* which is shown in Figure 4. The red/green curves show $\mu_0 H_A$ which includes the non-RE contribution to the MCA of the red/green plots in Fig. 3. Fig. 4 also shows the experimental measurements from Refs. [11, 42]. Below $T/T_c \sim 0.5$ there is some discrepancy between the two sets of experimental data, but above there is consistency between both the experiments and our calculations. The calculations show the clear importance of the Fe-dominated MCA to the anisotropy field at high temperatures - the red curve is over 1 T less than the green one over a range of temperatures despite the contributions from the non-RE MCAs differing by less than 30 μeV per Fe atom.

$Nd_2Fe_{14}B$'s spin reorientation transition (SRT) at 135K [8, 14, 43] is not described by our calculations owing to an underestimate of the high order crystal field coefficients [14, 44, 45]. This shortcoming exemplifies a more general challenge for theory modelling of low T strongly correlated f-electron effects to construct a robust way to significantly enhance the value of these coefficients [46]. Around room temperature and above, however, the ef-

fects on the MCA from these high order terms are small. This is also the temperature regime where the tenets of our DLM-DFT theory are valid.

$Nd_2Fe_{14}B$ and the RE-TM permanent magnet family to which it belongs have a compelling set of attributes. Their technological value is enormous and growing and their magnetic properties, at a fundamental level, come from a rich and subtle combination of RE, localized, and TM, itinerant electron, effects. To enhance magnetic functionality and extract pointers for the development of even better materials, multiple interrelated aspects have to be accounted for. Our *ab initio* DLM-DFT modelling has shown the importance of describing accurately the rich and complex itinerant electron magnetism associated with the Fe sites and valence electrons generally for the production of the robust exchange field acting on the RE atoms, the higher order effective spin interactions and the nature of the non-f electron MCA. The modifications proposed here should be incorporated into future atomistic, effective spin and micromagnetic modelling to correctly describe these phenomena.

---

* j.bouaziz@fz-juelich.de
† j.b.staunton@warwick.ac.uk

[1] R. J. Elliott, in *Magnetic Properties of Rare Earth Metals* (Plenum Press, London and New York, 1972) p. 2.

[2] J. M. D. Coey, Hard Magnetic Materials: A Perspective, IEEE Trans. Magn. **47**, 4671 (2011).

[3] S. Hirosawa, Preface to the viewpoint set on: Permanent magnets and underlining material science, Scripta Mat. **154**, 245 (2018).

[4] M. Richter, Band structure theory of magnetism in 3d-4f compounds, Journal of Physics D: Applied Physics **31**, 1017 (1998).

[5] M. D. Kuz'min and A. M. Tishin, Chapter three theory of crystal-field effects in 3d-4f intermetallic compounds, Handbook of Magnetic Materials **17**, 149 (2007).

[6] C. E. Patrick, M. Matsumoto, and J. B. Staunton, First-principles calculations of the magnetocrystalline anisotropy of the prototype 2:17 cell boundary phase $Y(Co_{1-x-y}Fe_xCu_y)_5$, Journal of Magnetism and Magnetic Materials **477**, 147 (2019).

[7] C. E. Patrick and J. B. Staunton, Temperature-dependent magnetocrystalline anisotropy of rare earth/transition metal permanent magnets from first principles: The light $RCo_5(R = $ Y,La-Gd) intermetallics, Phys. Rev. Materials **3**, 101401 (2019).

[8] J. F. Herbst, $R_2Fe_{14}B$ materials: Intrinsic properties and technological aspects, Rev. Mod. Phys. **63**, 819 (1991).

[9] See Supplemental Material for a picture of the crystal structure, site-resolved local, electronic spin-polarized densities of states, further information about multi-spin interactions, $Y_2Fe_{14}B$ magnetic properties, the 4f-atomic Hamiltonian and numerical values of magnetic in-

teractions between pairs of sites (see, also, references [47–53] therein).

[10] B. L. Gyorffy, A. J. Pindor, J. Staunton, G. M. Stocks, and H. Winter, A first-principles theory of ferromagnetic phase transitions in metals, Journal of Physics F: Metal Physics **15**, 1337 (1985).

[11] S. Hirosawa, Y. Matsuura, H. Yamamoto, S. Fujimura, M. Sagawa, and H. Yamauchi, Magnetization and magnetic anisotropy of $R_2Fe_{14}B$ measured on single crystals, Journal of applied physics **59**, 873 (1986).

[12] A. Liechtenstein, M. Katsnelson, and V. Gubanov, Exchange interactions and spin-wave stiffness in ferromagnetic metals, Journal of Physics F: Metal Physics **14**, L125 (1984).

[13] A. I. Liechtenstein, M. Katsnelson, V. Antropov, and V. Gubanov, Local spin density functional approach to the theory of exchange interactions in ferromagnetic metals and alloys, Journal of Magnetism and Magnetic Materials **67**, 65 (1987).

[14] Y. Toga, M. Matsumoto, S. Miyashita, H. Akai, S. Doi, T. Miyake, and A. Sakuma, Monte carlo analysis for finite-temperature magnetism of $Nd_2Fe_{14}B$ permanent magnet, Phys. Rev. B **94**, 174433 (2016).

[15] J. B. Staunton, L. Szunyogh, A. Buruzs, B. L. Gyorffy, S. Ostanin, and L. Udvardi, Temperature dependence of magnetic anisotropy: An ab initio approach, Phys. Rev. B **74**, 144411 (2006).

[16] C. E. Patrick and J. B. Staunton, Crystal field coefficients for yttrium analogues of rare-earth/transition-metal magnets using density-functional theory in the projector-augmented wave formalism, Journal of Physics: Condensed Matter **31**, 305901 (2019).

[17] J. P. Perdew and A. Zunger, Self-interaction correction to density-functional approximations for many-electron systems, Phys. Rev. B **23**, 5048 (1981).

[18] M. Lüders, A. Ernst, M. Däne, Z. Szotek, A. Svane, D. Ködderitzsch, W. Hergert, B. L. Györffy, and W. M. Temmerman, Self-interaction correction in multiple scattering theory, Phys. Rev. B **71**, 205109 (2005).

[19] C. E. Patrick and J. B. Staunton, Rare-earth/transition-metal magnets at finite temperature: Self-interaction-corrected relativistic density functional theory in the disordered local moment picture, Phys. Rev. B **97**, 224415 (2018).

[20] J. Cadogan and H.-S. Li, Analysis of the unusual temperature dependence of the anisotropy constant K_1 of $Y_2Fe_{14}B$, Journal of magnetism and magnetic materials **110**, L15 (1992).

[21] J. B. Staunton, R. Banerjee, M. d. S. Dias, A. Deak, and L. Szunyogh, Fluctuating local moments, itinerant electrons, and the magnetocaloric effect: Compositional hypersensitivity of FeRh, Phys. Rev. B **89**, 054427 (2014).

[22] E. Mendive-Tapia and J. B. Staunton, Ab initio theory of the gibbs free energy and a hierarchy of local moment correlation functions in itinerant electron systems: The magnetism of the mn$_3a$ materials class, Phys. Rev. B **99**, 144424 (2019).

[23] D. Boldrin, E. Mendive-Tapia, J. Zemen, J. B. Staunton, T. Hansen, A. Aznar, J.-L. Tamarit, M. Barrio, P. Lloveras, J. Kim, X. Moya, and L. F. Cohen, Multisite exchange-enhanced barocaloric response in Mn_3NiN, Phys. Rev. X **8**, 041035 (2018).

[24] E. Mendive-Tapia and J. B. Staunton, Theory of magnetic ordering in the heavy rare earths: Ab initio elec-

[25] E. Mendive-Tapia, D. Paudyal, L. Petit, and J. B. Staunton, First-order ferromagnetic transitions of lanthanide local moments in divalent compounds: An itinerant electron positive feedback mechanism and fermi surface topological change, Phys. Rev. B **101**, 174437 (2020).

[26] M. Matsumoto, R. Banerjee, and J. B. Staunton, Improvement of magnetic hardness at finite temperatures: Ab initio disordered local-moment approach for YCo_5, Phys. Rev. B **90**, 054421 (2014).

[27] C. E. Patrick, S. Kumar, G. Balakrishnan, R. S. Edwards, M. R. Lees, E. Mendive-Tapia, L. Petit, and J. B. Staunton, Rare-earth/transition-metal magnetic interactions in pristine and (Ni,Fe)-doped YCo_5 and $GdCo_5$, Phys. Rev. Materials **1**, 024411 (2017).

[28] C. E. Patrick and J. B. Staunton, MARMOT: magnetism, anisotropy, and more, using the relativistic disordered local moment picture at finite temperature, Electronic Structure (2022).

[29] J. Kuebler, magnetic moments of ferromagnetic and antiferromagnetic bcc and fcc iron, Physics Letters A **81**, 81 (1981).

[30] F. J. Pinski, J. Staunton, B. Gyorffy, D. D. Johnson, and G. M. Stocks, Ferromagnetism versus antiferromagnetism in face-centered cubic iron, Phys. Rev. B **56**, 2096 (1986).

[31] R. Cuadrado, R. F. Evans, T. Shoji, M. Yano, A. Kato, M. Ito, G. Hrkac, T. Schrefl, and R. W. Chantrell, First principles and atomistic calculation of the magnetic anisotropy of $Y_2Fe_{14}B$, Journal of Applied Physics **130**, 023901 (2021).

[32] R. F. Evans, L. Rózsa, S. Jenkins, and U. Atxitia, Temperature scaling of two-ion anisotropy in pure and mixed anisotropy systems, Physical Review B **102**, 020412 (2020).

[33] Y. Miura, H. Tsuchiura, and T. Yoshioka, Magnetocrystalline anisotropy of the fe-sublattice in $Y_2Fe_{14}B$ systems, Journal of Applied Physics **115**, 17A765 (2014).

[34] Q. Gong, M. Yi, R. F. L. Evans, B.-X. Xu, and O. Gutfleisch, Calculating temperature-dependent properties of $Nd_2Fe_{14}B$ permanent magnets by atomistic spin model simulations, Phys. Rev. B **99**, 214409 (2019).

[35] H. B. Callen and E. Callen, The present status of the temperature dependence of magnetocrystalline anisotropy, and the l(l+1)/2 power law, Journal of Physics and Chemistry of Solids **27**, 1271 (1966).

[36] C. E. Patrick, G. A. Marchant, and J. B. Staunton, Spin orientation and magnetostriction of $Tb_{1-x}Dy_xFe_2$ from first principles, Phys. Rev. Applied **14**, 014091 (2020).

[37] The jukkr developers, The Jülich KKR Codes (2020).

[38] N. Papanikolaou, R. Zeller, and P. H. Dederichs, Conceptual improvements of the KKR method, Journal of Physics: Condensed Matter **14**, 2799 (2002).

[39] C. E. Patrick, S. Kumar, G. Balakrishnan, R. S. Edwards, M. R. Lees, L. Petit, and J. B. Staunton, Calculating the magnetic anisotropy of rare-earth–transition-metal ferrimagnets, Phys. Rev. Lett. **120**, 097202 (2018).

[40] M. Loewenhaupt, I. Sosnowska, and B. Frick, Ground-state multiplet of rare-earth 3+ ions in $R_2Fe_{14}B$ investigated by inelastic neutron scattering, Phys. Rev. B **42**, 3866 (1990).

[41] M. Loewenhaupt and I. Sosnowska, Exchange and crystal

fields in $R_2Fe_{14}B$ studied by inelastic neutron scattering (invited), Journal of Applied Physics **70**, 5967 (1991).

[42] R. Grössinger, R. Krewenka, X. Sun, R. Eibler, H. Kirchmayr, and K. Buschow, Magnetic phase transitions and magnetic anisotropy in $Nd_2Fe_{14-x}Co_xB$ compounds, Journal of the Less Common Metals **124**, 165 (1986).

[43] M. Yamada, H. Kato, H. Yamamoto, and Y. Nakagawa, Crystal-field analysis of the magnetization process in a series of $Nd_2Fe_{14}B$-type compounds, Phys. Rev. B **38**, 620 (1988).

[44] K. Hummler and M. Fähnle, Full-potential linear-muffin-tin-orbital calculations of the magnetic properties of rare-earth–transition-metal intermetallics. ii. $Nd_2Fe_{14}B$, Phys. Rev. B **53**, 3290 (1996).

[45] Y. Tatetsu, Y. Harashima, T. Miyake, and Y. Gohda, Role of typical elements in $Nd_2Fe_{14}X$ (X = B, C, N, O, F), Phys. Rev. Materials **2**, 074410 (2018).

[46] L. V. Pourovskii, J. Boust, R. Ballou, G. G. Eslava, and D. Givord, Higher-order crystal field and rare-earth magnetism in rare-earth–Co_5 intermetallics, Phys. Rev. B **101**, 214433 (2020).

[47] O. Isnard, W. B. Yelon, S. Miraglia, and D. Fruchart, Neutron-diffraction study of the insertion scheme of hydrogen in $Nd_2Fe_{14}B$, Journal of Applied Physics **78**, 1892 (1995).

[48] Y.-K. Huang, C. Wu, Y. Chuang, F.-M. Yang, and F. De Boer, First-order magnetic transition in (nd, pr) 2fe14b, Journal of the Less Common Metals **132**, 317 (1987).

[49] F. Bolzoni, F. Leccabue, O. Moze, L. Pareti, M. Solzi, and A. Deriu, 3 d and 4 f magnetism in nd2fe14- x co x b and y2fe14- x co x b compounds, Journal of applied physics **61**, 5369 (1987).

[50] K. Stevens, Matrix elements and operator equivalents connected with the magnetic properties of rare earth ions, Proceedings of the Physical Society. Section A **65**, 209 (1952).

[51] J. Enkovaara, C. Rostgaard, J. J. Mortensen, J. Chen, M. Dułak, L. Ferrighi, J. Gavnholt, C. Glinsvad, V. Haikola, H. Hansen, *et al.*, Electronic structure calculations with gpaw: a real-space implementation of the projector augmented-wave method, Journal of physics: Condensed matter **22**, 253202 (2010).

[52] D. S. G. Bauer, Development of a relativistic full-potential first-principles multiple scattering Green function method applied to complex magnetic textures of nanostructures at surfaces, Forschungszentrum Jülich http://publications.rwth-aachen.de/record/229375 (2014).

[53] S. H. Vosko, L. Wilk, and M. Nusair, Accurate spin-dependent electron liquid correlation energies for local spin density calculations: a critical analysis, Canadian Journal of Physics **58**, 1200 (1980).